

Article

# Preparation and Performance Analysis of Nb Matrix Composites Reinforced by Reactants of Nb and SiC

Zhen Lu \*, Chaoqi Lan, Shaosong Jiang, Zhenhan Huang and Kaifeng Zhang

National Key Laboratory for Precision Heat Processing of Metals, Key laboratory of Micro-Systems and Micro-Structures Manufacturing Ministry of Education, Department of Materials Science and Engineering, Harbin Institute of Technology, Harbin 150001, China; xiayilcq@163.com (C.L.); jiangshaosong@hit.edu.cn (S.J.); huangfengzhenhan@163.com (Z.H.); kfzhang@hit.edu.cn (K.Z.)

\* Correspondence: luzhen-hit@163.com

Received: 5 February 2018; Accepted: 27 March 2018; Published: 3 April 2018



**Abstract:** In this paper, one kind of new composite material formed with Nb and SiC was prepared by hot pressing sintering. The influence of the addition of SiC particles on the mechanical properties at room and high temperature was analyzed. The composite material consists of three phases: Nb<sub>2</sub>C, Nb<sub>3</sub>Si, and Nb solid solution (Nbss). The fraction of SiC particles added in the Nb matrix was 3%, 5%, and 7%, respectively. Flexural strength, Vickers hardness, and compressive strength at room temperature were improved with the increasing of SiC content. Among them, compressive strength and fracture toughness were higher than those of Nb/Nb<sub>5</sub>Si<sub>3</sub> composites. The compressive strength at high temperature of the new composites was higher than that of Nb-Si alloys, which improved with the increasing of SiC content.

**Keywords:** Nb/SiC composite material; hot pressing sintering; microstructure; mechanical property

## 1. Introduction

In recent decades, greater demands have been placed on high-temperature structural materials with the rapid development of the aerospace field. At present, there are many high temperature metal materials that can be used under 1100 °C, including superalloy, TiAl intermetallic compound, titanium alloy, and others. Among them, the maximum service temperature of single crystal Ni-based superalloy is 1100 °C. On the other hand, there are some materials (W, Mo, Ta, Zr, Nb alloys) that can be used between 1100 °C and 2000 °C. The superhigh temperature materials still have a high strength at this temperature range. Ni-based alloys are most widely used in high-temperature components, but their operating temperature is close to the limiting temperature due to their melting point [1,2]. Refractory metals have received great attention because of their high melting point. Among the refractory metals, niobium alloy has the lowest density, and has attracted more attention from the public. In addition, Nb has stable physical and chemical properties, good corrosion resistance, and great ductility and machinability. Niobium alloy is expected to become a promising candidate for high-temperature applications [3].

Niobium alloy of Nb matrix composites are widely researched by scientists. The laminated Nb/Nb<sub>5</sub>Si<sub>3</sub> composites had been synthesized in situ by Yu et al. [4]. Nb<sub>5</sub>Si<sub>3</sub> phase was the reinforcement and Nbss had great plasticity, which could enhance the fracture toughness. In addition, Yu et al. [5] synthesized in situ Nb-silicide composite by powder metallurgy. Its nominal composition was Nb-16Si-10Ti-10Mo-5Hf. Solid solution strengthening and silicide hardening were the important strengthening mechanisms at high temperature. The reinforcements were Nb<sub>5</sub>Si<sub>3</sub> and a small amount of Nb<sub>3</sub>Si. Zhang et al. [6] studied the microstructure and properties of the Nb-Ti-C-Si system. The results indicated that borides and carbides effectively increased the strength and hardness of the composites,

while Nbss toughened the composites. Higher boron content increased the hardness and strength, but decreased the toughness. These studies show that the addition of reinforcements can significantly enhance the Nbss. The hardness of SiC particles is much higher than that of Si particles. Comparing to Si particles, the SiC particles are more easily surrounded by Nb particles. So, the mixed powders after ball milling are more uniform, the particles are finer and the structure of sintered material is more homogeneous. In addition, a study by Sha et al. [7] showed that Nb-based composites containing silicide and carbide phases had higher high-temperature yield strength and Vickers hardness than the composites with a single-silicide reinforced phase. There is little research on Nb-based materials reinforced by a mixture of carbide and silicide. Therefore, it is expected to produce a new type of composite with higher strength and better properties by adding SiC to the Nb solid solution. The vacuum melting method is the most common method to produce Nb-based composites [8,9]. However, composite materials produced by the vacuum melting method have shrinkage, poor density, and other defects. Beyond that, the reinforcements are prone to uneven distribution, which reduces the service performance of these materials. Hot pressing sintered materials have higher relative density and uniform structure [10]. However, research on preparing Nb-based composites with reinforcements of silicide and carbide phases is rare.

In the present study, Nb matrix composites reinforced by reactants of Nb and SiC (with SiC fractions of 3%, 5%, and 7%) were produced by hot pressing sintering technology. The effects of the amount of additional SiC on the microstructure and mechanical properties of composites were studied.

## 2. Experimental Procedure

Figure 1 shows the powder morphology of the original Nb and SiC powders, which was detected by scanning electron microscopy (SEM, FEI corporation, Hillsboro, OR, USA). It can be seen that the original Nb powders had irregular shape. The average particle size of Nb was 60  $\mu\text{m}$ , while the particle size of SiC powders was 2  $\mu\text{m}$ . The Nb-xSiC powders ( $x = 3\%$ , 5%, 7% molar ratio) were ball milled in a QM-BP planetary ball mill under Ar protective environment. The powders, weighing 30 g, were put together with steel balls. The ball-to-powder ratio was 15:1. In order to prevent the powder from welding during the ball milling, 20 mL ethanol was added to the pot. The ball milling time was 25 h and the speed was 250 r/min. The powders, after milling, were sintered at 1550  $^{\circ}\text{C}$  and 30 MPa for 1 h in the vacuum hot press sintering furnace. The sintered materials were marked as Nb-3SiC, Nb-5SiC, and Nb-7SiC.

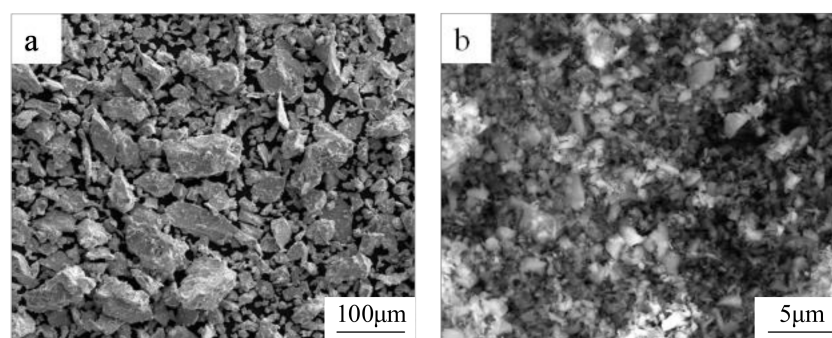


**Figure 1.** Morphology of original powders: (a) original Nb powders; (b) original SiC powders.

Samples were taken from the sintered materials for property testing and microstructure observation. Actual density was measured according to the Archimedean drainage method. Flexural strength and fracture toughness at room temperature were determined on the Instron-1186 universal testing machine. Flexural strength at room temperature was defined by a three-point bending test on specimens with 16 mm span length (total length = 20 mm), 4 mm width, and 3 mm thickness. Fracture toughness was determined by the single-edge notched beam three-point

bending test on specimens with 16 mm span length (total length = 20 mm), 4 mm width, 2 mm thickness, and a notch (2 mm depth). In the above two experiments, the loading speed of the pressing head was 0.5 mm/min, and the final result was the average value from five testing samples. Vickers hardness was measured on a MICRO-586 Vickers hardness tester with a load of 4 kg and a pressure of 15 s. The average hardness value was obtained from five indents on each sample.

High-temperature compression tests were performed on a Gleeble-1500D thermal simulation tester (DSI corporation, Poestenkill, NY, USA). The sample for testing was a cylinder with 4 mm diameter and 6 mm height, and the axis direction was the same as the hot pressing direction. Compression experiments were carried out at 1050 °C, 1100 °C, and 1150 °C. The strain rate was  $1 \times 10^{-3} \cdot \text{s}^{-1}$ . The deformation was 20% (true strain was 0.223), the heating rate was 20 °C/s, and the holding time was 20 s.

Scanning electron microscopy was used to observe the morphology of the powders during the different ball milling stages. Backscattered electron (BSE) images were produced to reveal the microstructure of the hot-pressed materials and high-temperature compressed samples. The samples were wire-cut from the material after hot-pressing and high-temperature compressing, then sanded with sandpaper. The final specimens were obtained by ion beam polishing. X-ray diffraction (XRD, Panalytical corporation, Almelo, Holland) was used to analyze the phase composition of the composite powders after milling and the sintered materials. Different stages of mechanically alloyed powders were placed on glass slides with square grooves, flattening these powders and determining the phase compositions. For sintered materials, after grinding and polishing the sintered block samples, the phase compositions were measured on the polished surface.

### 3. Results and Discussion

#### 3.1. Preparation of Nb/SiC Composite Powders

Ball milling has the benefit of obtaining a dense and uniform structure. By studying the micromorphology of composite powders, we can observe the refinement of powders and obtain the optimum milling time. Figure 2 shows the morphologies of composite powders with different ball milling times at a speed of 250 r/min. The morphology of the pure Nb powders after 20 h milling is shown in Figure 2a. The Nb particles were obviously refined into slices and sticks in comparison with the initial powders (10–20 μm). As shown by red arrows in Figure 2a, cracks formed in the Nb powders. After adding SiC and ball milling for 25 h, the powders were obviously refined. Most of the powders were in the form of crumbs (3–4 μm), and the particles were evenly distributed. Continuing milling to 30 h, Nb powders were not further refined.

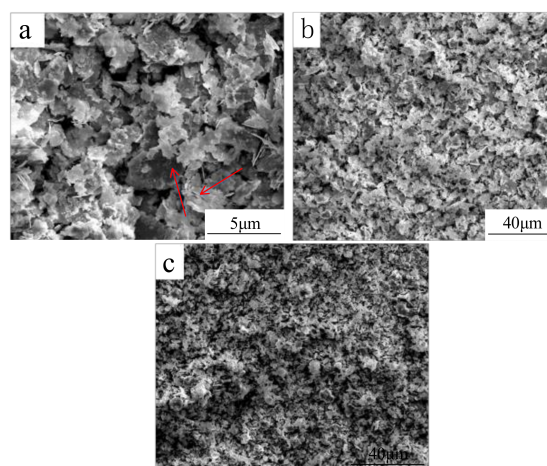


**Figure 2.** Scanning electron microscope micrographs of Nb/SiC composite powders ball milled for (a) 20 h; (b) 25 h; (c) 30 h.

The results of XRD analysis of Nb and SiC powders milled for different times are shown in Figure 3. Compared with the XRD patterns of the original Nb powders, it can be seen that the diffraction peaks of Nb powders became broader and the intensities decreased when the Nb powders were milled for 25 h. This is because Nb powders undergo strong plastic deformation during the milling process, which causes lattice distortions and increased dislocation, resulting in an increased amount of subgrains and an area of subgrain boundaries [11]. When the number of subgrains increases to a certain extent, the subgrains will transform into grains so that the grains will be refined. Grain refinement and lattice distortion will lead to broadening diffraction peaks. Meanwhile, grain refinement can also lead to reducing diffraction peak intensity [12].

When powders were milled for 30 h, the secondary peak showed in the left of the main peak of Nb powders, indicating that the main diffraction peaks of Nb powders began to move toward the direction of low angle and the lattice constant of Nb powders increased [13]. This is because the iron element inevitably enters the composite powders during ball milling because of the stainless-steel balls and cans used. The atomic radius of Fe is 1.72 Å and the atomic radius of Nb is 2.08 Å. If an Fe atom enters the lattice interstices of Nb to form an interstitial solid solution, the lattice constant of Nb will increase and the diffraction peak will shift toward the lower angle. As shown in Figure 3, the diffraction peak width of Nb powders does not increase significantly from 25 to 30 h, indicating that the particle size of Nb powders does not change significantly during this process. In addition, the longer the milling time, the more impurities will be introduced. Based on the above analysis, 25 h is the optimal milling time.

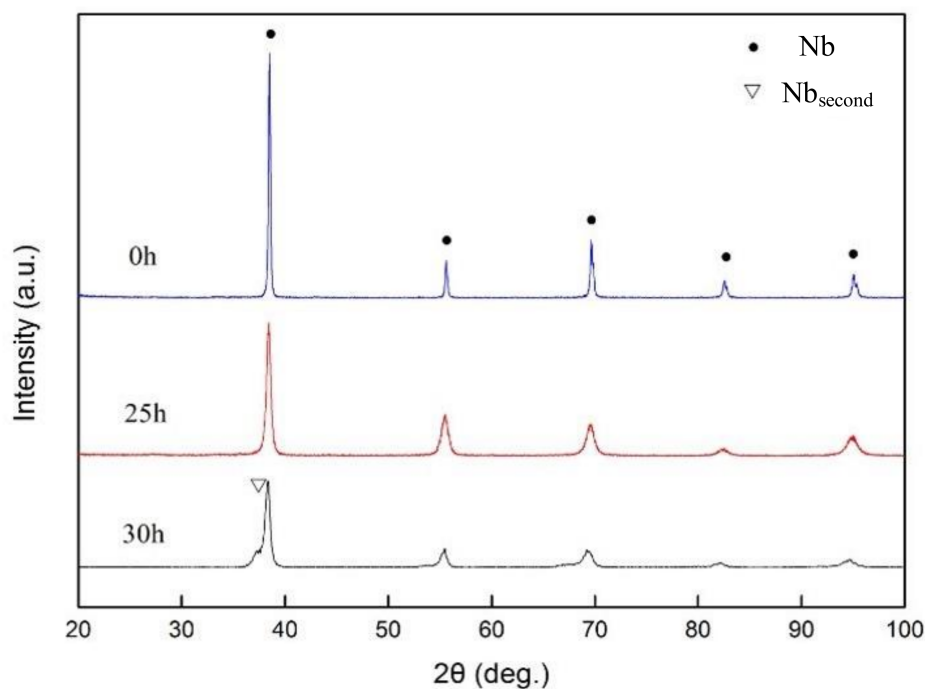


**Figure 3.** X-ray diffraction (XRD) patterns of composite powders after different milling times.

Figure 4 shows the XRD patterns of three composite powders after ball milling for 25 h. It can be seen from the figure that no diffraction peak of SiC was detected. This is because at the initial stage of ball milling, Nb particles turn into sheets due to plastic deformation. The brittle SiC powders not only have little content, but also have small particle size (generally no more than 2 μm). The SiC powder particles are easily broken into particles that are less than 1 μm under the high-speed impact of the ball. Only a few SiC powders embed into Nb powders. Pressing composite powders and making

samples for the XRD test at this time, the flaky Nb particles will cover small SiC particles, which makes it difficult to detect the diffraction peak of SiC.

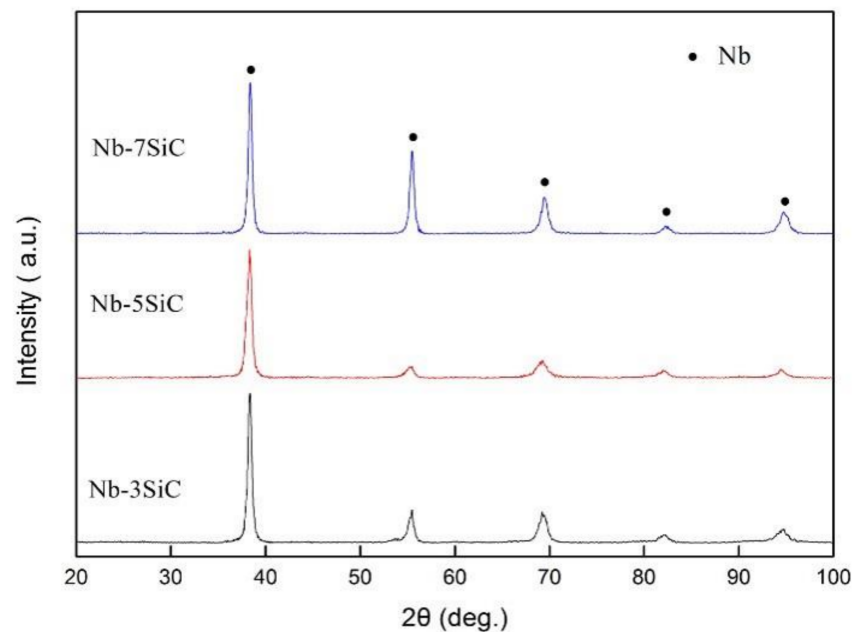


**Figure 4.** XRD patterns of composite powders after milling for 25 h.

### 3.2. Microstructure and Mechanical Properties at Room Temperature

#### 3.2.1. XRD Patterns and Microstructure of Sintered Material

XRD patterns of the sintered materials are shown in Figure 5. Compared with the XRD pattern of the milled composite powders, a new phase was formed in the sintered materials. The diffraction peaks of  $\text{Nb}_3\text{Si}$ ,  $\text{Nbss}$ , and  $\text{Nb}_2\text{C}$  can be detected in the XRD patterns of the three kinds of sintered materials. The diffraction peaks of Nb-Si intermetallic compound were not detected in the XRD pattern after ball milling for 25 h (Figure 3). Therefore, the Nb-Si intermetallic compound found in the sintered materials was generated by the reaction of Nb and SiC in the hot pressing process. Sintered materials consisted of three phases:  $\text{Nbss}$ ,  $\text{Nb}_3\text{Si}$ , and  $\text{Nb}_2\text{C}$ . Comparing the XRD patterns of the three composites, the diffraction peak of  $\text{Nbss}$  was strongest and the area the peak covered was the largest, indicating that there was the most content of  $\text{Nbss}$  in three phases, and the three composite materials were based on  $\text{Nbss}$ .

Figure 6 shows BSE images of the three kinds of composite. The material was dense, and the grains were more refined with increasing SiC content. The average grain size of Nb-3SiC was 10  $\mu\text{m}$ , the average crystal size of Nb-5SiC was 8  $\mu\text{m}$ , and the average grain size of Nb-7SiC was 4  $\mu\text{m}$ . The composite materials consisted of three contrasting phases of black, gray, and white. It was known from the XRD patterns that the material consisted of  $\text{Nb}_2\text{C}$ ,  $\text{Nb}_3\text{Si}$ , and  $\text{Nbss}$  phases. Generally it is well known that phases containing heavier elements exhibit brighter contrast in BSE images, thus the black grains are  $\text{Nb}_2\text{C}$ , the white grains are  $\text{Nbss}$ , and the gray grains are  $\text{Nb}_3\text{Si}$ . From the image it can be observed that the black grains were always adjacent to the gray grains, indicating that SiC particles react with the surrounding  $\text{Nbss}$  during hot press sintering. C and Si atoms diffuse locally: C atoms diffuse into the black grains, and Si atoms diffuse into the gray grains. The original Si and C atoms are adjacent, so the  $\text{Nb}_2\text{C}$  and  $\text{Nb}_3\text{Si}$  grains produced by the reaction are also adjacent, which proves that the black grains are also  $\text{Nb}_2\text{C}$ . In addition, certain areas in  $\text{Nb}_2\text{C}$  were darker in color, indicating that C was locally enriched in these regions and was unevenly distributed in the  $\text{Nb}_2\text{C}$  grains.

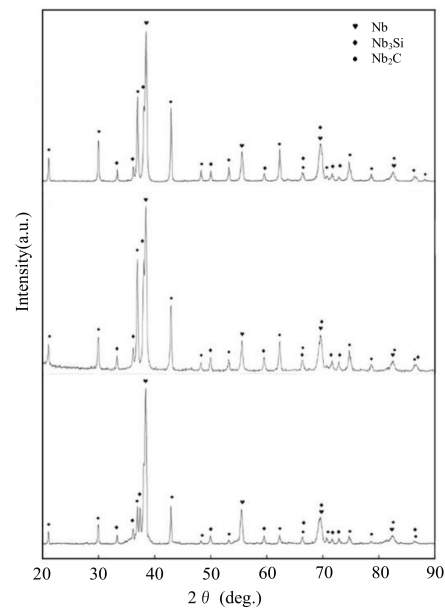


Figure 5. XRD patterns of Nb-xSiC composites.

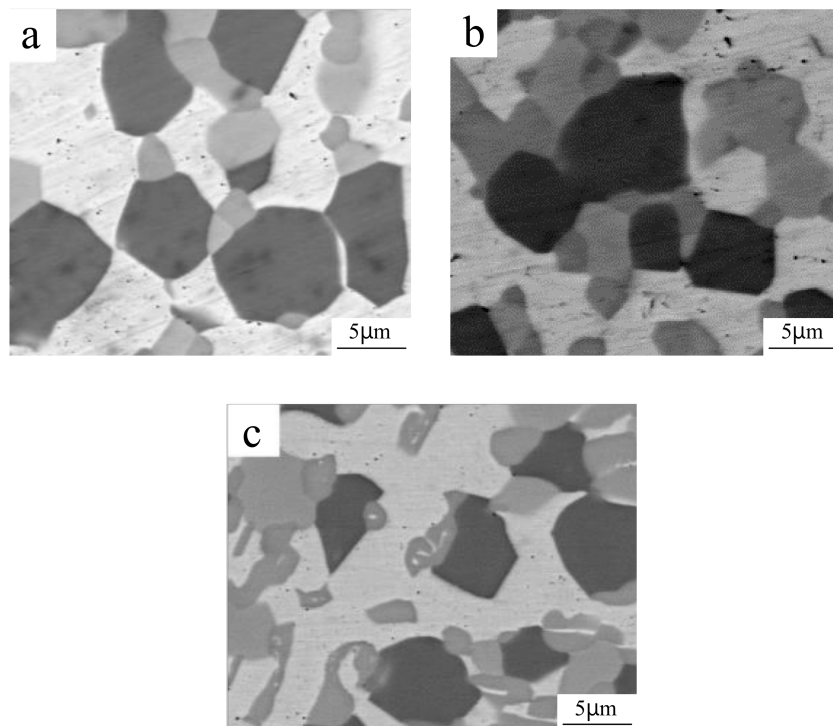


Figure 6. Backscattered electron images of the three composites: (a) Nb-3SiC; (b) Nb-5SiC; (c) Nb-7SiC.

### 3.2.2. Mechanical Properties of Nb Matrix Composites at Room Temperature

Adding SiC to Nbss, mixed reinforcement consisting of carbide and silicide would be produced, which made it possible to give the Nbss better mechanical properties at room temperature. Figure 7a shows the room temperature flexural strength and fracture toughness of the new Nb matrix composites obtained with different amount of SiC. It can be seen from the figure that flexural strength increased with the addition of SiC. Flexural strength of the three components was 754.52 MPa, 793.63 Mpa, and 814.38 Mpa, respectively. The reason is that the content of Nb<sub>2</sub>C and Nb<sub>3</sub>Si formed by the reaction

increased with the addition of SiC. Nb<sub>2</sub>C and Nb<sub>3</sub>Si, which are both hard and brittle phases, embed into Nbss, hindering the movement of dislocation during deformation and having the function of dispersion hardening. The fracture toughness of the new Nb matrix composites decreased with the addition of SiC. The fracture toughness of the three materials was 13.82 MPa<sup>1/2</sup>, 12.74 MPa<sup>1/2</sup>, and 11.37 MPa<sup>1/2</sup>, respectively. Nb/Nb<sub>5</sub>Si<sub>3</sub> composites have been widely studied by researchers. The room temperature fracture toughness of Nb was 3MPa<sup>1/2</sup> [14], and it could go up to 8 MPa<sup>1/2</sup> of Nb/Nb<sub>5</sub>Si<sub>3</sub> composites. The room temperature fracture toughness of Nb and Nb/Nb<sub>5</sub>Si<sub>3</sub> composites were both lower than that of the new Nb matrix composites. Figure 7b shows the room temperature compressive strength and Vickers hardness of composites with different amounts of SiC. Compressive strength and Vickers hardness both increased with the amount of SiC. The compressive strength of the three materials was 1659 MPa, 1780 MPa, and 1915 MPa, respectively. The Vickers hardness was 567 HV, 601 HV, and 623 HV, respectively. The compressive strength of Nb/Nb<sub>5</sub>Si<sub>3</sub> composites was 1400 MPa. It can be seen that the compressive strength of the new Nb matrix composites improve greatly compared with Nb/Nb<sub>5</sub>Si<sub>3</sub> composites.

Figure 8a shows the Vickers indentations of the new Nb matrix composites with different amounts of SiC. It can be seen from the figure that cracks existed only in the Nb<sub>2</sub>C and Nb<sub>3</sub>Si grains and ended at the grain boundary of Nbss, also known as crack arrest (CA). Cracks passed through the hard and brittle phases in the manner of transgranular fractures (TF) [15] and deflected when the cracks propagated. The Nbss phase is ductile. When a crack propagates in the Nbss, it undergoes plastic deformation, which consumes the energy required for crack propagation during deformation and applies compressive stress to the tip of a crack to close it. Finally, it offsets tensile stress at the tip and slows the propagation of the crack. With the increasing of SiC content, the content of the Nbss phase reduces relatively and the fracture toughness decreases. Besides, there are a greater number of grains (smaller grain size) in the same volume with the increasing of SiC content. So during the deformation process, the deformation that disperses to each grain is smaller. Thus, it is difficult to form cracks in grains. Macroscopically, the material can withstand large deformation without breaking quickly. In addition, with the increasing of SiC content, the grain boundary surface area increases. It hinders the movement of dislocations during deformation. Meanwhile, the amounts of Nb<sub>2</sub>C and Nb<sub>3</sub>Si increase and strengthen the Nbss, so the compressive strength increases with the increasing of SiC content. Furthermore, the increase of Nb<sub>2</sub>C and Nb<sub>3</sub>Si also augments the number of hard and brittle phases in the indentation area, resulting in increasing hardness.

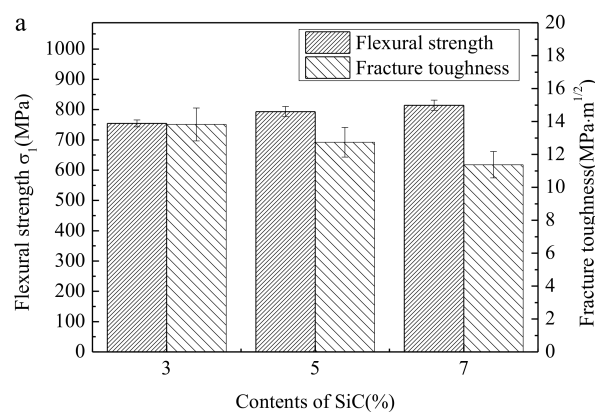
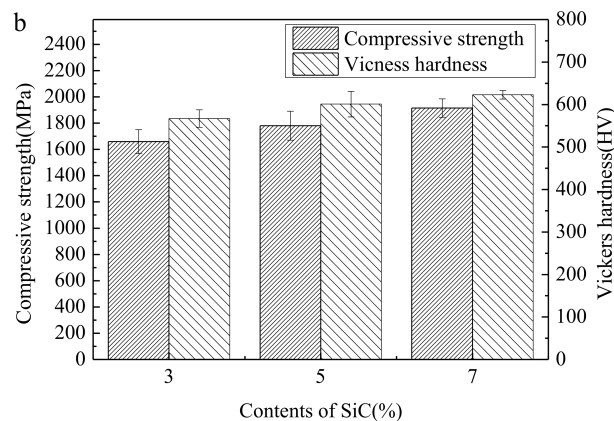
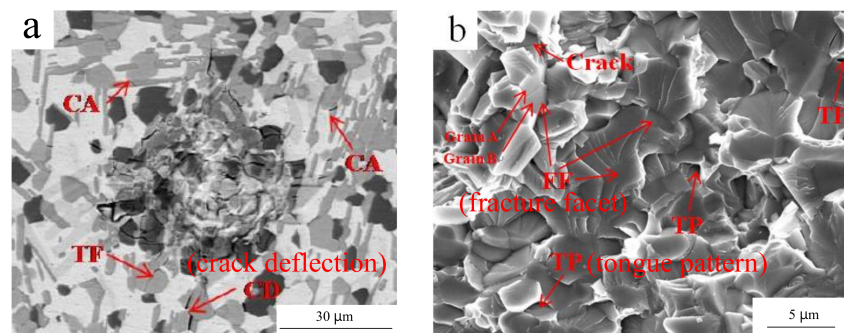


Figure 7. Cont.



**Figure 7.** Room temperature mechanical properties of the new Nb matrix composites: (a) flexural strength and fracture toughness; (b) compressive strength and Vickers hardness.

Figure 8b shows the fracture morphology of an Nb-5SiC specimen after the three-point bending test. As the figure shows, Nb<sub>2</sub>C exhibited a transgranular cleavage fracture mode, inlaid into the Nbss like skeletons. In the process of flexural fracture, Nb<sub>2</sub>C gradually bends when it suffers bending load. When deformation reaches a certain extent, the cracks begin to germinate, and they propagate inside the Nb<sub>2</sub>C grains, which is known as transgranular fracture. The more SiC is added, the more Nb<sub>2</sub>C forms, and the greater the load suffered during the deformation process. Besides, in the process of propagation, cracks continually change direction, which virtually slows the crack growth rate, delaying fracture. Therefore, the room temperature flexural strength of composites increased with the amount of SiC.

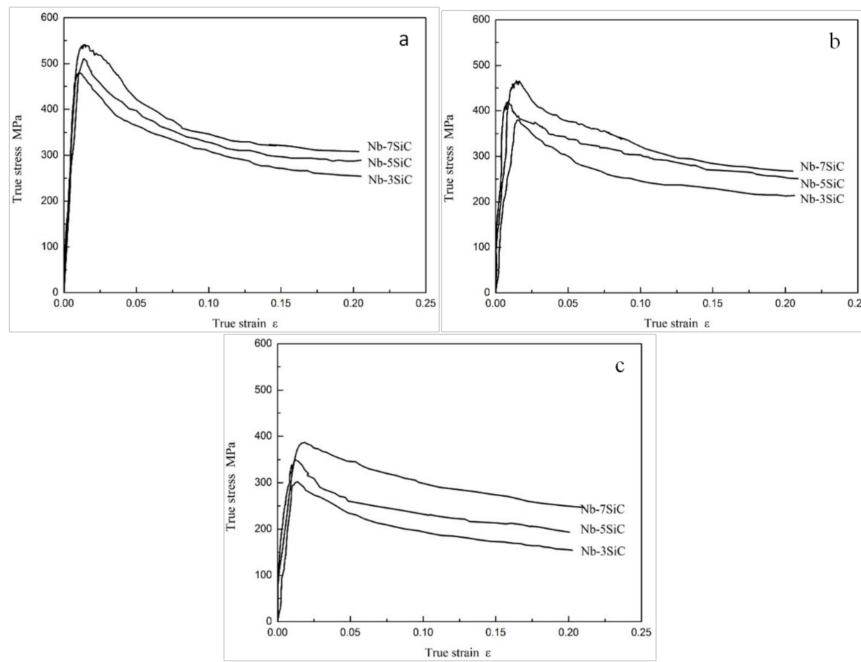


**Figure 8.** Vickers hardness indentation and fracture morphology of composites: (a) Vickers hardness indentation; (b) fracture morphology.

### 3.3. Behavior of Nb Matrix Composites at High Temperature

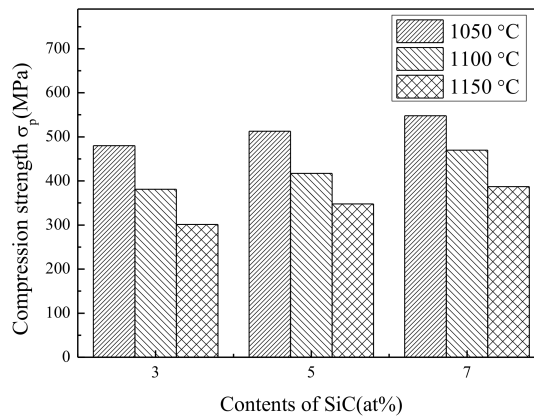
#### 3.3.1. Stress-Strain Curve at High Temperature

Figure 9 shows the true stress-strain curves of the three materials at 1050 °C, 1100 °C, and 1150 °C. When compression started, there was an increase in flow stress as dislocations interacted and multiplied, and the true stress grew extremely fast. When it reached the peak, the true stress declined gradually. When the dislocation density increased to a certain degree, dynamic restoration occurred. The climb of edge dislocations, cross-slip of screw dislocations and counteraction of unlike dislocations are basic to the softening mechanism of the dynamic recovery, which contributes to lowering the dislocation density and opening dislocation tangle. Meanwhile, the rate of dislocation migration accelerates with increasing temperature, which decreases the deformation resistance [16]. Thus, the slope of the flow stress curve slowed down gradually.



**Figure 9.** True stress-strain curves of the three materials at different temperatures: (a) 1050 °C; (b) 1100 °C; (c) 1150 °C.

Figure 10 shows the compressive strength of the three materials at 1050 °C, 1100 °C, and 1150 °C. It can be observed that with the increasing of SiC, compressive strength gradually increases. Compressive strength of the three materials at 1050 °C was 480 MPa, 513 Mpa, and 548 MPa. Compressive strength at 1100 °C was 381 MPa, 417 Mpa, and 470 MPa, respectively. When the temperature was 1150 °C, compressive strength was 301 MPa, 348 Mpa, and 387 MPa for the three materials, respectively. Introducing Hf, Cr, and other elements into the Nb-Si alloys could improve the mechanical properties of the Nb-Si alloys. Compressive strength of the 0Hf-2B-3Cr-54Nb-22Si-based alloy and the 2Hf-2B-3Cr-52Nb-22Si-based alloy at 1250 °C was 194 MPa and 291 Mpa [17], respectively; compressive strength of Nb-8Si-20Ti-6Hf-(6,10,14)Cr at 1150 °C was 268 MPa, 278 Mpa, and 313 MPa [18]. The compressive strength of ordinary Nb-Si alloys was lower than that of the new Nb matrix composites, which shows that the addition of SiC could significantly improve the high-temperature strength of the material.



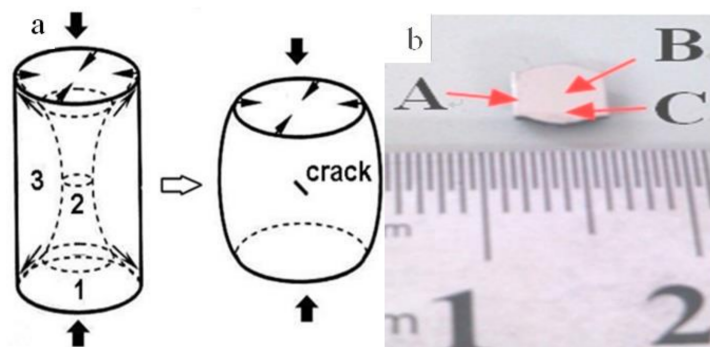
**Figure 10.** Compressive strength and peak stress at different temperatures.

With the increase of added SiC, deformation resistance and compressive strength of the material increased and the Nbss was strengthened. This is because, as the content of SiC increases, Nb<sub>2</sub>C and Nb<sub>3</sub>Si increase, and the bonding areas with Nbss also increase, hindering the movement of dislocation during deformation. In addition, the hard and brittle phases are of great help for second-phase strengthening, which also improves the high-temperature strength of the material.

### 3.3.2. Microstructure of Material after High-Temperature Deformation

During the compression process, the specimen was divided into three parts. As shown in Figure 11a, zone 1 is the dead zone, with the least deformation, zone 2 is the pressure zone, with the largest deformation, and zone 3 is the tension stress zone. The corresponding areas on the actual compression specimen are shown in Figure 11b, a longitudinal cross-sectional view of the compressed specimen. The three regions indicated by the arrows labeled A, B, and C in Figure 11b correspond to the regions labeled 1, 2, and 3 shown in Figure 11a.

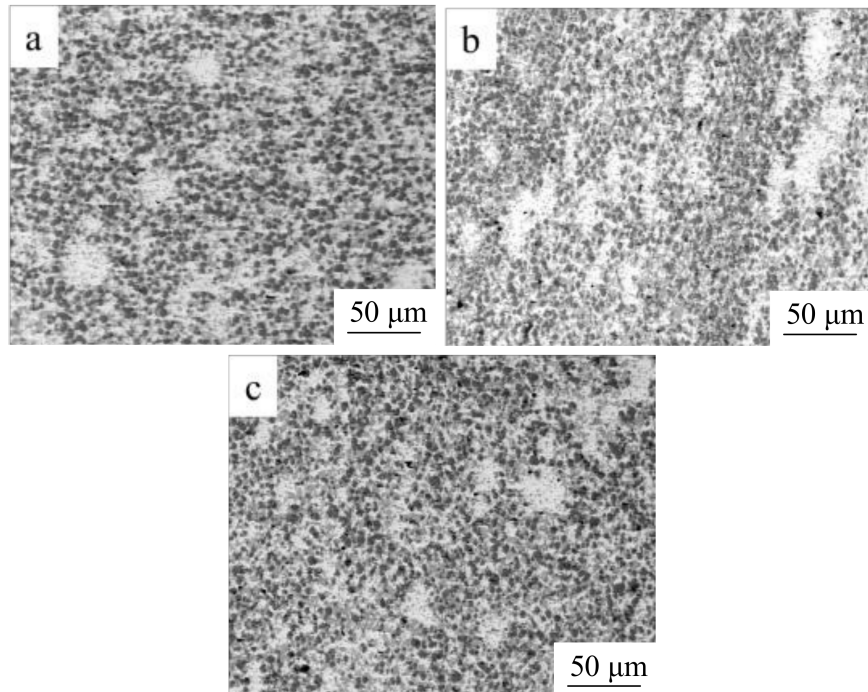
Figure 12a–c show the BSE images corresponding to the three regions A, B, and C, respectively, in Nb-5SiC (Figure 11b). The area shown in Figure 12a is close to the pressing head and belongs to the undeformed area, retaining the equiaxed grain structure of original tissue. Figure 12b is the deformation area of the compression sample. The middle part of the equiaxed grain structure was squashed, showing a strip-shaped structure. Compared with the A region, the morphology of the C region did not have significant changes, because the total compression deformation was small and the deformation in the C region was smaller, resulting in insignificant changes of the tissue.



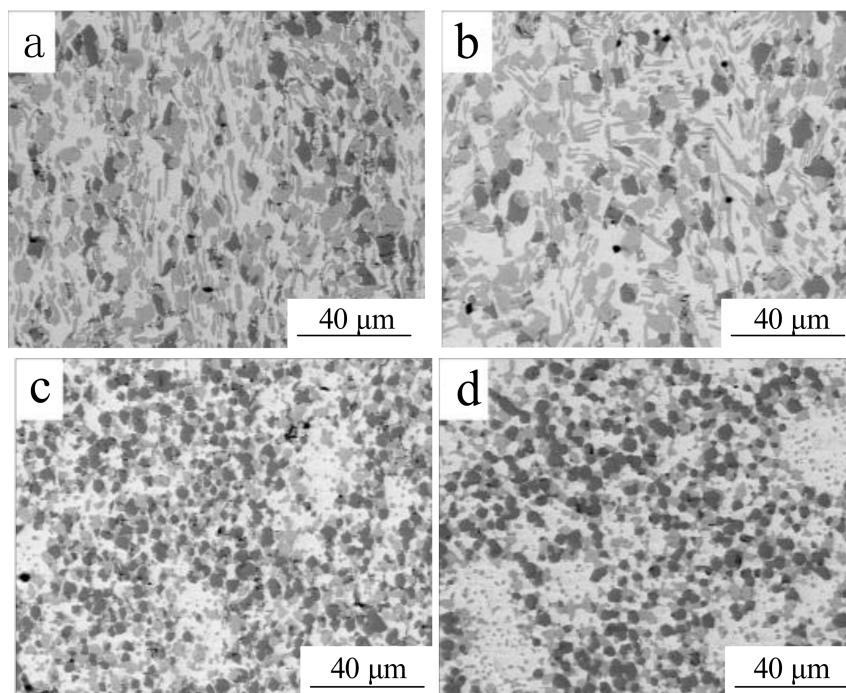
**Figure 11.** Stress states of different parts in the compressive sample: (a) schematic diagram; (b) actual sample.

Figure 13 shows BSE images of the deformed area B in the middle of Nb-5Si and area C after deformation at different temperatures. There was a common feature among these diagrams: cracks existed in grain boundaries between Nb<sub>2</sub>C and Nb<sub>3</sub>Si, but there were no cracks in the grain boundaries between hard, brittle phases and Nbss. This is because with increased deformation, there is inconsistent deformation between Nb<sub>2</sub>C and Nb<sub>3</sub>Si, so that cracks occur in the grain boundaries. However, the deformation between the hard brittle phases and the ductile Nbss is coordinate, and thus it is not easy to produce cracks. This indicates that the material is about to undergo intergranular fracture, while the fracture mode of the material is transgranular cleavage fracture at room temperature. The maximum load of material at room temperature was greater than at high temperature. This is because at room temperature, the grain boundary strength is high and the intragranular strength is low, so the fracture mode is mainly transgranular fracture. Meanwhile, because of the small grain size of the material, the grain boundary not only impedes dislocation, but also withstands large deformation, so that it is difficult to crack. Therefore, the material has good plasticity and high strength at room temperature. As the temperature increases, the grain boundary strength and intragranular strength both decrease, but the strength of the grain boundary decreases more, resulting in the transformation of transgranular fracture at room temperature to intergranular fracture at high temperature. Because of

the low grain boundary strength at high temperature, the material will crack with small deformation. However, the ductile Nbss can absorb the energy of crack growth and delay crack propagation, playing a significant role in improving deformation of the material and preventing premature fracture.



**Figure 12.** Backscattered electron images of different parts of Nb-5SiC at 1050 °C: (a) zone A; (b) zone B; (c) zone C.



**Figure 13.** Cont.

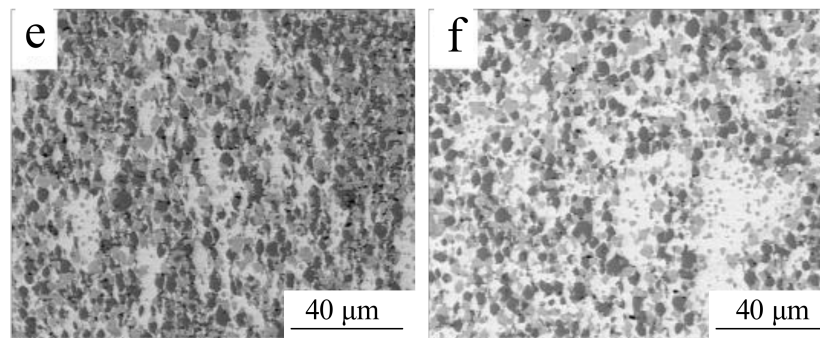


**Figure 13.** Backscattered electron images of Nb-5Si at different temperatures: (a) zone B at 1050 °C; (b) zone C at 1050 °C; (c) zone B at 1100 °C; (d) zone C at 1100 °C; (e) zone B at 1150 °C; (f) zone C at 1150 °C.

#### 4. Conclusions

1. The new Nb matrix composites were prepared by hot pressing sintering process. The reinforcements consisted of Nb<sub>2</sub>C, Nb<sub>3</sub>Si, and Nbss. The relative density of material sintered was 97%, indicating that the material had good compactness.
2. At room temperature, the flexural strength of Nb-3SiC, Nb-5SiC, and Nb-7SiC composites was 754.52 MPa, 793.63 MPa, and 814.38 MPa, respectively. The fracture toughness was 13.82 MPa<sup>1/2</sup>, 12.74 MPa<sup>1/2</sup>, and 11.37 MPa<sup>1/2</sup>, respectively. Compressive strength was 1659 MPa, 1780 MPa, and 1915 MPa, respectively. Vickers hardness was 567 HV, 601 HV, and 623 HV, respectively. The performance was better than that of Nb/Nb<sub>5</sub>Si<sub>3</sub> composites (fracture toughness = 8 MPa<sup>1/2</sup>, compressive strength = 1400 MPa).
3. The compressive strength of Nb-3Si, Nb-5Si, and Nb-7Si was 480 MPa, 513 MPa, and 548 MPa, respectively, at 1050 °C. The compressive strength of Nb-7Si at 1050 °C, 1100 °C, and 1150 °C was 584 MPa, 470 MPa, and 387 MPa, respectively. In addition, the high-temperature compressive strength of composite materials was higher than that of ordinary Nb-Si alloys.

**Acknowledgments:** The authors gratefully acknowledge financial support from the National Natural Science Foundation of China (grant No. 51675126) and the Natural Science Foundation of Heilongjiang Province (grant No. DC2013C048).

**Author Contributions:** Zhen Lu designed this experiment and revised the manuscript. Chaoqi Lan analyzed the experimental data and completed this paper. Zhenhan Huang performed the nanoindentation experiments. Shaosong Jiang and Kaifeng Zhang helped to complete the microstructure analysis.

**Conflicts of Interest:** The authors declare no conflict of interest.

#### References

1. Xu, Y.; Sun, W.; Dai, W.; Hu, C.; Liu, X.; Zhang, W. Experimental and numerical modeling of the stress rupture behavior of nickel-based single crystal superalloys subject to multi-row film cooling holes. *Metals* **2017**, *7*, 340. [[CrossRef](#)]
2. Rodríguez-Millán, M.; Díaz-Álvarez, J.; Bernier, R.; Cantero, J.L.; Rusinek, A.; Miguelez, M.H. Thermo-viscoplastic behavior of ni-based superalloy haynes 282 and its application to machining simulation. *Metals* **2017**, *7*, 561. [[CrossRef](#)]
3. Lei, R.; Wang, M.; Xu, S.; Wang, H.; Chen, G. Microstructure, hardness evolution, and thermal stability mechanism of mechanical alloyed Cu-Nb alloy during heat treatment. *Metals* **2016**, *6*, 194. [[CrossRef](#)]
4. Yu, C.; Zhao, X.; Xiao, L.; Cai, Z.; Zhang, B.; Guo, L. Microstructure and mechanical properties of in-situ laminated Nb/Nb<sub>5</sub>Si<sub>3</sub> composites. *Mater. Lett.* **2017**, *209*, 606–608. [[CrossRef](#)]
5. Yu, J.; Weng, X.D.; Zhu, N.; Liu, H.; Wang, F.; Li, Y.; Cai, X.; Hu, Z. Mechanical properties and fracture behavior of an nb-silicide in situ composite. *Intermetallics* **2017**, *90*, 135–139. [[CrossRef](#)]

6. Zhang, X.; He, X.; Fan, C.; Li, Y.; Song, G.; Sun, Y.; Huang, J. Microstructural and mechanical characterization of multiphase nb-based composites from Nb-Ti-C-B system. *Int. J. Refract. Met. Hard Mater.* **2013**, *41*, 185–190. [[CrossRef](#)]
7. Sha, J.; Hirai, H.; Tabaru, T.; Kitahara, A.; Ueno, H.; Hanada, S. Effect of carbon on microstructure and high-temperature strength of Nb Mo Ti Si in situ composites prepared by arc-melting and directional solidification. *Mater. Sci. Eng. A* **2003**, *343*, 282–289. [[CrossRef](#)]
8. Geng, J.; Tsakiroopoulos, P. A study of the microstructures and oxidation of Nb-Si-Cr-Al-Mo in situ composites alloyed with ti, hf and sn. *Intermetallics* **2007**, *15*, 382–395. [[CrossRef](#)]
9. Geng, J.; Tsakiroopoulos, P.; Shao, G. A study of the effects of hf and sn additions on the microstructure of Nbss/Nb<sub>5</sub>Si<sub>3</sub> based in situ composites. *Intermetallics* **2007**, *15*, 69–76. [[CrossRef](#)]
10. Nassef, A.; El-Garaihy, W.H.; El-Hadek, M. Characteristics of cold and hot pressed iron aluminum powder metallurgical alloys. *Metals* **2017**, *7*, 170. [[CrossRef](#)]
11. Wang, X.; Wang, G.; Zhang, K. Effect of mechanical alloying on microstructure and mechanical properties of hot-pressed Nb-16Si alloys. *Mater. Sci. Eng. A* **2010**, *527*, 3253–3258. [[CrossRef](#)]
12. Jayasankar, K.; Pandey, A.; Mishra, B.; Das, S. Evaluation of microstructural parameters of nanocrystalline Y<sub>2</sub>O<sub>3</sub> by X-ray diffraction peak broadening analysis. *Mater. Chem. Phys.* **2016**, *171*, 195–200. [[CrossRef](#)]
13. Wang, X.; Zhang, K. Mechanical alloying, microstructure and properties of Nb-16Si alloy. *J. Alloy. Compd.* **2010**, *490*, 677–683. [[CrossRef](#)]
14. Zhang, L.; Wu, J. Ti5Si3 and Ti5Si3-based alloys: Alloying behavior, microstructure and mechanical property evaluation. *Acta Mater.* **1998**, *46*, 3535–3546. [[CrossRef](#)]
15. Gulizzi, V.; Rycroft, C.; Benedetti, I. Modelling intergranular and transgranular micro-cracking in polycrystalline materials. *Comput. Methods Appl. Mech. Eng.* **2018**, *329*, 168–194. [[CrossRef](#)]
16. Jiang, S.Y.; Zhang, Y.Q.; Zhao, Y.N. Dynamic recovery and dynamic recrystallization of NiTi shape memory alloy under hot compression deformation. *Trans. Nonferrous Metals Soc. China* **2013**, *23*, 140–147. [[CrossRef](#)]
17. Zhang, S.; Guo, X. Effects of B addition on the microstructure and properties of Nb silicide based ultrahigh temperature alloys. *Intermetallics* **2015**, *57*, 83–92. [[CrossRef](#)]
18. Sha, J.; Yang, C.; Liu, J. Toughening and strengthening behavior of an Nb-8Si-20Ti-6Hf alloy with addition of Cr. *Scr. Mater.* **2010**, *62*, 859–862. [[CrossRef](#)]



© 2018 by the authors. Licensee MDPI, Basel, Switzerland. This article is an open access article distributed under the terms and conditions of the Creative Commons Attribution (CC BY) license (<http://creativecommons.org/licenses/by/4.0/>).